STUDY ON INFLUENCE OF FORCED VIBRATION OF COOLING CHANNEL ON FLOW AND HEAT TRANSFER OF HYDROCARBON FUEL AT SUPERCRITICAL PRESSURE

by

Mantang CHEN[a], Yin HU[b], Zhixiong HAN[c], Zilong PENG[b], and Hao ZAN[b*]

[a] Beijing Power Machinery Institute, Beijing, China
[b] Jiangsu University of Science and Technology, Jiangsu, China
[c] Harbin Institute of Technology, Heilongjiang, China

Original scientific paper
https://doi.org/10.2298/TSCI210706267C

The cooling channel of a scramjet is the fundamental structure of the active thermal protection for an engine. Till now, studies have focused mainly on the steady-state flow and heat transfer process in the cooling channel. However, the vibration intensity of an engine increases sharply as the flight speed increases, because of which, the flow and heat exchange mechanisms based on the cooling channel under stable conditions cannot be applied under vibration. In this study, experimental methods are used to study the characteristics of the forced vibration of a cooling channel on the flow and heat transfer of hydrocarbon fuel at supercritical pressure. In addition, the influences of different vibration frequencies and vibration amplitudes on the flow and heat transfer are analyzed. The research results show that at supercritical pressure, when the fuel temperature is below the critical temperature and the inner wall temperature is above the critical temperature, external vibrations would enhance the heat transfer characteristics of the cooling channel. However, when the pressure and temperature are unstable, the forced vibration of the cooling channel would suppress the instability of temperature and pressure while strengthening the heat exchange.

Key words: *cooling channel, forced vibration, hydrocarbon fuel, flow heat exchange, unstable flow*

Introduction

Hypersonic flight technology has been of high importance to the aerospace field in this century. An air-breathing hypersonic flight vehicle refers to an aircraft that has a flight Mach number of at least five. It is powered by an air-breathing scramjet engine [1-4]. However, the high Mach number of scramjet engines causes a severe problem with regard to thermal protection. When the flight speed attains a Mach number of six, the aerodynamic heating and combustion heat release cause the peak heat flux in the combustion chamber to attain 3 MW/m^2. This causes the central flow temperature of the combustion chamber to attain a value in the range of 2500-3000 K [5]. Regenerative cooling is considered to be one of the most effective cooling methods for preventing the degradation in quality that results from carrying additional coolant [6]. The hydrocarbon fuel functions as a coolant in the cooling

* Corresponding author, e-mail: zanhao870127@163.com

channel and a fuel in the combustion chamber. This strong coupling necessitates fuel flow control. The fuel is first supplied to the pipe-line through the fuel pump. Then, its flow rate is calibrated using a flow meter. In the fuel supply system, a differential pressure flow meter is generally used for flow calibration. However, this set-up may cause unstable flow and interfere with the regulation of the fuel supply system [7]. In severe cases, it may cause high temperature ablation of the engine wall, difficulty in fuel flow control, and vibration damage to the mechanical structure.

Chinese and foreign researchers have carried out substantial research on hydrocarbon fuel flow oscillations. Bi *et al.* [8] observed carried out a heat transfer experiment with supercritical kerosene in the micro-channel. They observed that the heat transfer would deteriorate and sound oscillation would be produced when the temperature of the working fluid is lower than the pseudo-critical temperature and the pipe wall temperature is higher than this temperature. Kafengauz and Fedorov [9] observed that the heat transfer of pseudo-boiling is accompanied by pressure oscillations. Linne *et al.* [10] conducted a heat transfer experiment on JP-7 and observed that flow oscillations occurred in all the experiments at supercritical pressure. Zhou *et al.* [11] considered that the variations in the physical properties of fuel in the pseudo-critical region and during pyrolysis are the main factors that cause the flow oscillation. It was also observed [12-15] that the flow oscillation in the cooling channel is caused by thermoacoustic instability. These studies focused mainly on the flow oscillation phenomenon in the heating process of the cooling channel. There are few research studies on the flow oscillation problem in the flow measurement process at the cold end.

Scramjet has a simple structure with stringent restrictions on the structural quality. Although it generally has a thin-walled structure, it should be capable of withstanding substantial aerodynamic loads and aerodynamic thermal loads. Therefore, combustion oscillation is an important cause of wall vibration [16, 17]. Wall vibration has a substantial influence on the flow characteristics of the fluid in the pipes, which can occasionally become unstable [18]. Soong *et al.* [19] conducted an experimental study on convective heat transfer in a rotating radial square isothermal pipe. The flow and heat transfer phenomenon are affected by the secondary flow generated by Coriolis force and buoyancy, whereas the strength of the secondary flow depends on the rotational Reynolds number. Benhamou *et al.* [20] studied the dynamic process of an incompressible fluid in a swinging horizontal pipe. The local axial velocity and local wall shear stress when the pipe vibrates are less than those without vibration. The fluid characteristics of a horizontal pipe with low frequency cyclic vibration were also investigated [21]. Cyclic secondary flow phenomenon was observed in the fluid inside the pipe. Xie *et al.* [22] studied the complex interaction between structure and internal flow dynamics, obtained a phase diagram of the transition between different phases, and summarized the types of fluid motion induced by the flow pattern in the pipe. Mittal *et al.* [23] proposed a stable finite element method to perform a global non-parallel flow stability analysis for a 2-D steady-state flow with marginal disturbances. Thereby, they formulated the criteria for distinguishing between stability and instability.

Few studies in the published literature have been carried out on the influence of vibration on the flow and heat transfer of hydrocarbon fuel in the cooling channel, particularly the influence on the unstable flow and heat transfer in the critical region. This study mainly investigates the influence of vibration on the heat transfer characteristics of the cooling channel. Special attention is paid to the dynamic effect of external vibration on the pseudo-critical and critical zones.

Experimental system and data processing

Experimental system

A high temperature fuel electric heating and vibration experimental system was established to study the forced vibration of the cooling channel in the flow and heat transfer process of hydrocarbon fuel. The fuel used was RP-3 aviation kerosene. The system structure is shown in fig. 1. The hydrocarbon fuel flows out of the fuel tank through the constant-flux pump. To prevent the pump from being blocked and damaged by impurities, a 40 μm filter is installed between the fuel tank and the pump. The fuel flows into the mass-flow meter through the shut-off valve and the insulating device and then, into the heating section after flow measurement at the flow meter. Ceramic square tubes are used to bridge the two ends of the heating section, and the vibration exciter is used to ensure that the heating section vibrates only in one direction. Twenty six thermocouples are uniformly arranged on the outer wall of the heating section measure the temperature of the outer wall.

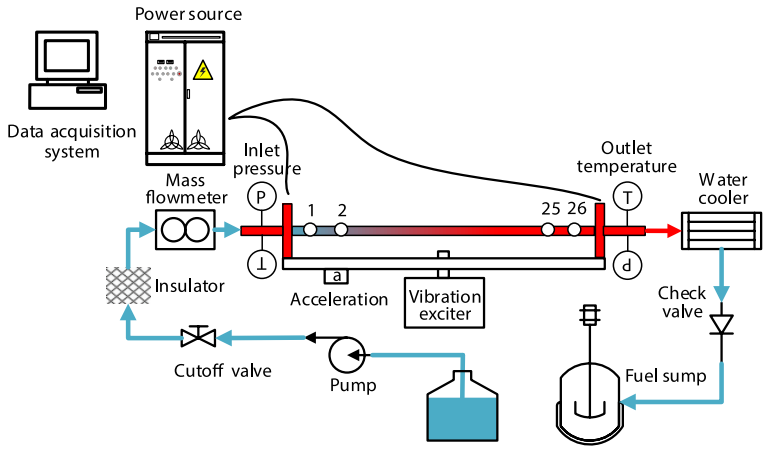

Figure 1. Diagram of high temperature electric heating/vibration experimental system for hydrocarbon fuel

The fuel enters the heat recovery system after passing through the test tube (or observation section). This is to enable the study of the influence of external vibration on the flow and heat transfer of the cooling channel. The experimental system has the following specifications. The power cabinet adopts a stabilized DC power supply with a maximum power of 6 kW. The plunger pump used is the SP1020 high pressure infusion pump manufactured by Shanghai Sanotac Scientific Instruments Co., Ltd., which has a pressure resistance of 25 MPa. The mass-flow is measured with the E series CMF010 flowmeter manufactured by Micro Motion from Emerson Electric Co. USA. It has a maximum measurable flow of 108 kg/h and pressure resistance of 40 MPa. The fluid temperature is measured with a *K*-type armored thermocouple with a diameter of 0.3 mm. To improve the response speed of the fuel temperature, the head of the armored thermocouple needs to be ground off to reduce the heat capacity of the thermocouple. The pressure is measured with a pressure transmitter having a measurement range of 10 MPa manufactured by Microsensor Co., Ltd., Shaanxi Province, China. The data acquisition system is manufactured by the National Instruments Corporation, USA. The vibration exciter is of the DH40100 type manufactured by Donghua Testing Technology Co., Ltd. It has a maximum excitation force of 100 N and frequency range between 0.1 Hz and 2.5 kHz. The vibration exciter also uses the DH5872 amplifier from Donghua Testing Technology Co., Ltd., which has a

rated output power of 200 W and frequency range of DC ~40 kHz. The signal generator is the DH1301 generator manufactured by Donghua Testing Technology Co., Ltd. The accelerometer is the 1A316E three-way accelerometer, which is also manufactured by Donghua Testing Technology Co., Ltd. It has a sensitivity of ~5 mV/(m/s^2) and measurement range of 1000 m/s^2. An axial vibration of approximately 10 Hz would cause the pipe to swing up and down, which would make it unfeasible to guarantee that the heating section moves only in the axial direction. Therefore, the heating section is fixed on the guide rail to restrict its movement in other directions. There is no swinging movement in other directions during radial vibration, whereby it is unnecessary to restrict the position of the heating section by the sliding rail device.

Data processing

In this paper, the heat transfer characteristics refer to:

– the variations in the local heat transfer coefficient or Nusselt number according to the fuel temperature with or without external vibration and
– influence of parameters such as system pressure, heat flux, flow rate, vibration direction, vibration frequency, and vibration amplitude on these variations.

Data acquisition can be achieved through direct measurement and indirect measurement. In this experiment, direct measurement is used to capture data directly through sensors, including parameters such as flow, pressure, inlet fuel temperature, voltage, current, outer wall temperature, and vibration acceleration. Meanwhile, indirect measurement is used to obtain certain physical quantities that cannot be measured conveniently or certain variables with theoretical values. Because these values cannot be measured, these need to be calculated from directly measured quantities. The methods to obtain the indirectly measured heat transfer coefficient and Nusselt number from the directly measured parameters are introduced in this section.

The local heat transfer coefficient is expressed:

$$h_x = \frac{q_x}{T_{\mathrm{wx,in}} - T_{\mathrm{b},x}} \tag{1}$$

where q_x is the local wall heat flux density, $T_{\mathrm{wx,in}}$ – the local inner wall temperature, and $T_{\mathrm{b},x}$ – the local fuel temperature.

The local Nusselt number is calculated:

$$\mathrm{Nu}_x = \frac{h_x d_i}{\lambda_x} \tag{2}$$

where d_i is the inner diameter of the test tube and λ_x – the local thermal conductivity of kerosene. The directly measured physical quantities in the experiment include the fuel inlet temperature, T_{in}, fuel outlet temperature, T_{out}, fuel inlet flow rate, $\dot{m}$, outer-wall temperature measurements, $T_{\mathrm{wo},x}$ of 26 points arranged uniformly along the heating section, outlet pressure, P, of the test tube, heating voltage, U, of the test tube, and heating current, I. To obtain heat transfer characteristics including the local heat transfer coefficient and Nusselt number, it is necessary to derive the local heat flux, q_x, local inner wall temperature, $T_{\mathrm{wi},x}$, and local fuel temperature, $T_{\mathrm{b},x}$ from these directly measured physical quantities.

Assuming that the heating section has a length, L, and the current flowing through the heating section is I, the local heat flux is calculated:

$$q_x = \frac{I^2 R_x}{\pi d_{\mathrm{in}} L} - q_{\mathrm{loss},x} \tag{3}$$

where R_x is the resistance of the control body, d_{in} – the inner diameter of the test tube, and $q_{\mathrm{loss},x}$ – the local heat dissipation density. The resistance R_x of the stainless steel tube:

$$R_x = \frac{4\rho_x L}{\pi\left(d_{\text{out}}^2 - d_{\text{in}}^2\right)} \tag{4}$$

where ρ_x is the resistivity of stainless steel and d_{out} – the outer diameter of the test tube. Substituting eq. (4) into eq. (3):

$$q_x = \frac{4I^2\rho_x}{\pi d_{\text{in}}\left(d_{\text{out}}^2 - d_{\text{in}}^2\right)} - q_{\text{loss},x} \tag{5}$$

Equation (5) is the formula to calculate the local heat flux density from known quantities. Here, the resistivity, ρ_x, of the stainless steel is a function of the local outer-wall temperature, $T_{\text{wo},x}$. The local heat dissipation density, $q_{\text{loss},x}$, is related to the surface characteristics and size of the heat dissipation surface and the temperature difference with the environment. When the size of the test tube and ambient temperature are constant, the heat dissipation density is a function of only the outer wall temperature, $T_{\text{wo},x}$. These two functions can be obtained by calibration prior to the experiment. Thus, eq. (5) shows that the local heat flux density is a function of the current flowing through the test tube, inner and outer diameters of the test tube, and local outer-wall temperature. After the outer wall temperature is measured, the inner wall temperature can be calculated using the formula for the heat transfer in a 1-D pipe with an internal heat source.

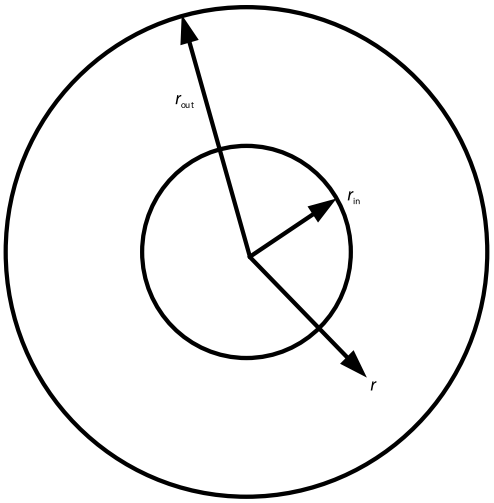

Figure 2. Schematic diagram of local inner wall temperature calculation

The schematic diagram of local inner wall temperature calculation is shown in fig. 2. The thermal differential equation of tube:

$$\frac{1}{r}\frac{\partial}{\partial r}\left(\lambda_{\text{s}} r\frac{\partial T}{\partial r}\right) + \dot{\Phi} = 0 \tag{6}$$

$$\dot{\Phi} = \frac{I^2 R(T)}{\pi^2\left(r_{\text{out}}^2 - r_{\text{in}}^2\right)} \tag{7}$$

where λ_{s} is the thermal conductivity of stainless steel and $\dot{\Phi}$ – the volumetric heat source. The boundary conditions are such that when $r = r_{\text{out}}$, $T = T_{\text{wo},x}$, and $\lambda_{\text{s}} = \partial T/\partial r = -q_{\text{loss},x}$. Therefore, the inner wall temperature is obtained by integrating from r_{in} to r_{out}. The formula for calculating the inner wall temperature

$$T_{\text{wx,in}} = \frac{\left(T_{\text{wx,out}} - \dot{\Phi}\frac{r_{\text{out}}^2}{2} - q_{x,\text{loss}} r_{\text{out}}\right)\ln\frac{r_{\text{out}}}{r_{\text{in}}} - \frac{\dot{\Phi}}{4}\left(r_{\text{out}}^2 - r_{in}^2\right)}{k_x} \tag{8}$$

Equation (8) is the formula for calculating the local inner-wall temperature. It is evident that the inner wall temperature is determined by the current flowing through the heating

section, inner and outer diameters of the heating section, local outer wall temperature, and thermal conductivity of stainless steel. Because the pipes in the heating section used in this experiment are thin-walled, the temperature difference between the inner and outer walls of the pipe is marginal, and the temperature gradient in the radial direction of the stainless steel material is moderate. Therefore, the thermal conductivity corresponding to the outer wall temperature is used while calculating the thermal conductivity of stainless steel.

The heat dissipation capability of the pipe to the surrounding air can be calibrated by the air heating experiment. The pipe is filled with still air at normal pressure and then heated. When the system is at equilibrium, because there is no convective heat transfer, the power delivered by the power supply to the heating pipe is equal to the power lost by the heating pipe to the outside air. It is assumed that at this time, the area influenced by the axial heat conduction at both ends of the heating pipe is limited. Therefore, the average temperature of the middle section of the heating pipe is considered. Because of the axial heat conduction, the temperatures at the left and right ends of the heating pipe are lower than that of the middle section. The average temperature of the middle section is considered as the temperature of the entire pipe. That is, in the absence of axial heat conduction at both ends of the heating pipe, the temperature at these ends is approximately equal to this average temperature [24, 25]. The fitting curve can be expressed in the form of a polynomial function:

$$\dot{q}_{\text{loss}}\left(T_{\text{wo}}\right)=\frac{UI}{A_{jh}}=a\left(T_{\text{wo}}-T_0\right)^3+b\left(T_{\text{wo}}-T_0\right)^2+c\left(T_{\text{wo}}-T_0\right)+d \tag{9}$$

where $q_{\text{loss}}(T_{\text{wo}})$ [Wm^{-2}] is the heat flux density of the heat dissipation loss of the heating pipe, T_{wo} [°C] – the temperature of the outer wall of the pipe, A_{jh} [m^2] – the outer surface area of the heating pipe, and T_0 [°C] – the ambient temperature. Similar to the inner wall temperature, the fuel temperature inside the heating section cannot be measured directly and is hence estimated. Curve fitting is performed with the total heat sink of the fuel along the entire pipe length and the fuel outlet fuel temperature to obtain:

$$\dot{Q}_{\text{total}}=f\left(\overline{T}_{\text{out}}\right)=a\overline{T}_{\text{out}}^4+b\overline{T}_{\text{out}}^3+c\overline{T}_{\text{out}}^2+d\overline{T}_{\text{out}}+e \tag{10}$$

where $\overline{T}_{\text{out}}$ [°C] is the outlet fuel temperature of the heating section. Because the thermocouple measures the average temperature of the cross-section, it is indicated by the bar on the symbols. According to the fitted curve, the average temperature of the working fluid in the pipe can be inverse calculated according to the heat sink at a certain local position:

$$\overline{T}_f=f^{-1}\left(\dot{Q}_{\text{total}}\right) \tag{11}$$

Uncertainty analysis

The heating section has a length of 500 mm, an inner diameter of 2 mm, and a wall thickness of 0.5 mm. The two ends of the heating section are connected with the electrode, and the pipe is heated by adjusting the electric power at both ends of the electrode. The 26 thermocouples are uniformly welded 20 mm apart on the wall of the heating section. The flow and heat transfer characteristics in the pipe are calculated mainly by the temperatures obtained from the 26 thermocouples on the pipe wall, the mainstream temperature of the fuel oil at the inlet and outlet, and the inlet and outlet pressure. Therefore, the precision of the temperature and pressure data measurement is highly important.

Table 1. Uncertainty of direct measurement data

Measurement parameter	Equipment	Precision
Outer wall temperature [K]	*K*-type thermocouple	±0.5 K
Fuel temperature [K]	Armored thermocouple	±0.5 K
Inner diameter [mm]	Scanning electron microscope	±0.0005
Mass-flow rate [gs^{-1}]	Coriolis flowmeter	±0.15%
Voltage [V]	Voltmeter	±0.2%
Current [A]	Ammeter	±0.2%

The process of uncertainty analysis refers to the [26]. The uncertainties of the experimental data measured directly are shown in tab. 1. Because the temperature difference between the inner and outer walls is within 2 K, the uncertainty of the inner wall temperature is determined to be 1.05 K under all the experimental conditions:

$$\left|\frac{\delta(\Delta T)}{\Delta T}\right| = \frac{\sqrt{\left|\delta T_{wx,in}\right|^2 + \left|\delta T_{bx}\right|^2}}{30} = 4.7\% \tag{12}$$

Because total heat flux and heat loss are two independent variables, the following uncertainties can be obtained according to the error propagation formula:

$$\left|\frac{\Delta q_x}{q_x}\right| = \sqrt{\left(\frac{q_x + q_{loss}}{q_x}\right)^2 \varepsilon^2\left(q_{0,x}\right) + \left(\frac{q_{loss,x}}{q_x}\right)^2 \varepsilon^2\left(q_{loss,x}\right)} \tag{13}$$

The uncertainty of the total heat flux:

$$\left|\frac{\Delta q_x}{q_x}\right| = \sqrt{4\varepsilon^2(I) + \left(\frac{2d_{out}^2}{d_{out}^2 - d_{in}^2}\right)^2 \varepsilon^2\left(d_{out}\right) + \left(\frac{2d_{in}^2}{d_{out}^2 - d_{in}^2}\right)^2 \varepsilon^2\left(d_{in}\right) + \varepsilon^2\left(d_{out}\right)} = 1.37\% \tag{14}$$

Therefore, the uncertainty of heat loss:

$$\left|\frac{\Delta q_{loss,x}}{q_{loss,x}}\right| = \sqrt{\varepsilon^2(U) + \varepsilon^2(I) + \varepsilon^2\left(d_{out}\right) + \varepsilon^2(L) + \varepsilon^2\left(T_{wx,out}\right)} = 0.85\% \tag{15}$$

When the ratio of heat loss to effective heat flux is less than 5%, the value of eq. (13) is 1.53%. The uncertainty of the heat transfer coefficient can be obtained through the aforementioned derivation:

$$\left|\frac{\Delta h_x}{h_x}\right| = \sqrt{\varepsilon^2\left(q_x\right) + \varepsilon^2(\Delta T)} = \sqrt{(1.53\%)^2 + (4.7\%)^2} = 4.93\% \tag{16}$$

Based on the aforementioned measurement results, the uncertainty of the thermal conductivity of hydrocarbon fuel is within 3% and that of the inner diameter is 0.46%. Therefore, the maximum uncertainty of Nusselt number can be determined:

$$\left|\frac{\Delta \mathrm{Nu}_x}{\mathrm{Nu}_x}\right| = \sqrt{\varepsilon^2\left(h_x\right) + \varepsilon^2(\lambda) + \varepsilon^2\left(d_{in}\right)} = \sqrt{(4.93\%)^2 + (3.0\%)^2 + (0.46\%)^2} = 5.8\% \tag{17}$$

Experimental results and analysis

Influence of vibration on stable flow heat transfer

To prevent film boiling during the cooling process of the fuel, the pressure in the channel at the hot end is generally higher than the supercritical pressure of the fuel. The fuel would experience three thermodynamic phases as the temperature increases: the subcritical, pseudo-critical, and supercritical zones. Its physical properties would vary dramatically during this process. Under the condition of supercritical pressure, the fuel density and isobaric specific heat capacity vary most dramatically in the subcritical temperature region and across the critical temperature region. When the system enters the supercritical region completely, the variation in these physical properties slows down gradually. The characteristics of this variation in physical properties cause the hydrocarbon fuel to show a variety of flow field characteristics in the temperature region before pyrolysis occurs.

To study the influence of external vibration on the heat transfer characteristics of the hot-end channel under supercritical pressure conditions, the working conditions were set with a pressure of 4 MPa, a mass-flow rate of 0.55 g/s, and an inlet temperature of 293 K. Figures 3 and 4 describe the influence of radial vibration on the heat transfer coefficient along the pipe with heating powers of 70 W/m^{2}K and 140 W/m^{2}K, respectively. When the heating power is 70 W/m^{2}K, external vibrations of different frequencies and various acceleration amplitudes have negligible effects on the heat transfer coefficient. When the heating power is 140 W/m^{2}K, the external vibration exerts a substantial influence on the heat transfer coefficient at the rear end of the pipe. Vibrations with different frequencies and amplitudes have different influences on the heat transfer coefficient. The higher the frequency, the larger is the increase in heat transfer coefficient. But the increase in vibration amplitude changes both the value of the transmission and the location of this increase.

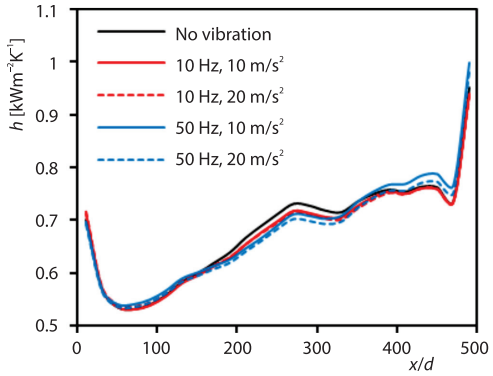

Figure 3. Variations of heat transfer coefficient along the flow direction (70 W/m^{2}K)

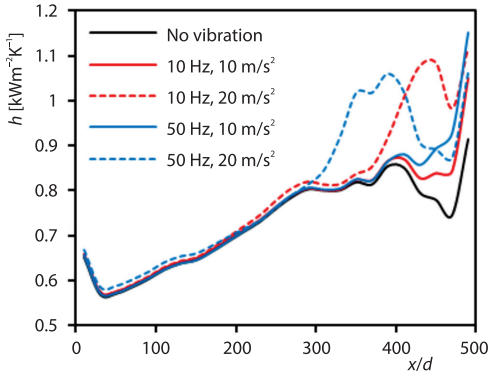

Figure 4. Variations of heat transfer coefficient along the flow direction (140 W/m^{2}K)

Under identical conditions of external vibration, different heating powers yield different heat transfer characteristics. This is because the increase in heating power alters the temperature of the fuel and thereby, alters the thermophysical properties of the fuel. Figures 5 and 6 show the variations in the main flow temperature and boundary-layer temperature along the flow direction under different heat flux conditions. It is observed that with a heating power of 70 W/m^{2}K or 140 W/m^{2}K, the temperature of the main flow along the flow direction is less

than the pseudo-critical temperature, and the thermal properties of the main flow undergo negligible variations. In contrast, for an identical heating power, the boundary-layer fuel temperature is approximately equal to the inner wall temperature. The results are shown in figs. 3 and 4. When the heating power is 70 W/m^{2}K, the boundary-layer fuel temperature is less than the pseudo-critical temperature in a subcritical zone. At this time, the fuel physical properties vary negligibly. This indicates that vibration has negligible influence on the heat transfer coefficient. When the heating power is 140 W/m^2·K, the boundary-layer fuel temperature displays values in the subcritical zone, pseudo-critical zone, and supercritical zone in the direction of flow. It is observed that vibration exerts an influence on the fuel in the supercritical zone. This would cause the temperature in the supercritical zone of the fuel in the boundary-layer to decrease and thereby, enhance the heat transfer in this area.

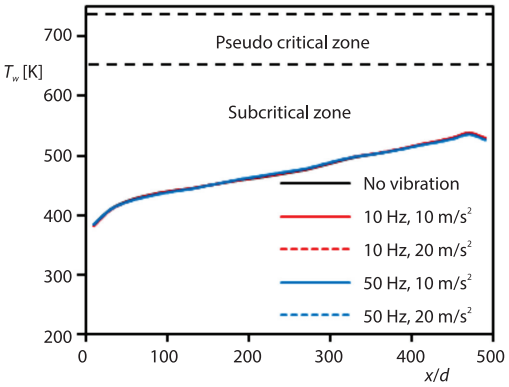

Figure 5. Variations of inner wall temperature along the flow direction (70 KW/m^{2}K)

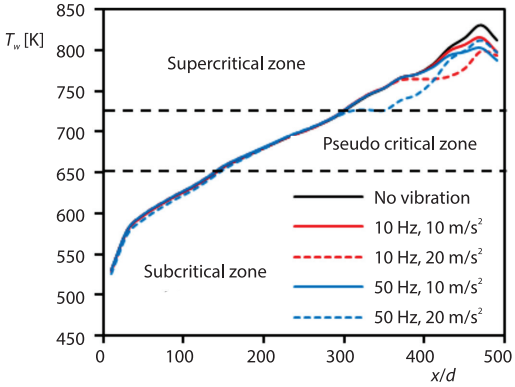

Figure 6. Variations of inner wall temperature along the flow direction (140 KW/m^{2}K)

The variations in the heat transfer coefficient and inner wall surface temperature along the flow direction for a pressure of 5 MPa, mass-flow rate of 1.5 g/s, and heating power of 80 kW/m^{2}K are shown in figs. 7 and 8. When the vibration frequency is 10 Hz, the vibration has negligible influence on the heat transfer. When the vibration frequency is 50 Hz, the vibration

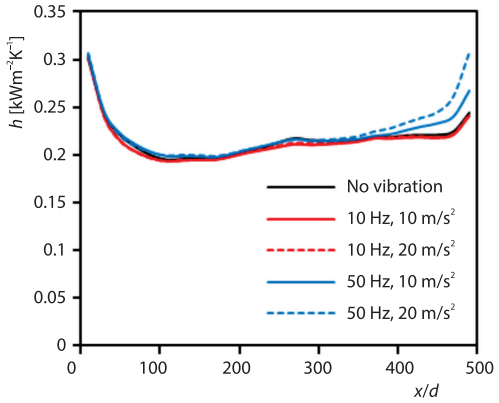

Figure 7. Variations of heat transfer coefficient along the flow direction (80 W/m^{2}K)

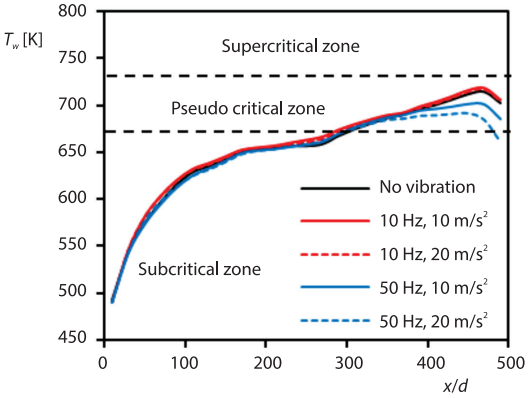

Figure 8. Variations of inner wall temperature along the flow direction (80 W/m^{2}K)

causes an increase in the heat transfer coefficient of the section adjacent to the outlet. Because the main flow temperature is below 500 K, which is significantly lower than the critical temperature, the main flow thermophysical properties vary negligibly. In contrast, the fuel temperature of the boundary-layer is in the critical zone at the section next to the outlet. This is consistent with the enhanced heat transfer zone caused by vibration. Therefore, it is inferred that an external vibration with a certain frequency disturbs the boundary-layer fuel with a temperature in the pseudo-critical zone. This can result in a decrease in the wall temperature and thereby, enhance the heat transfer.

The variations in the heat transfer coefficient and inner wall surface temperature along the flow direction for a pressure of 5 MPa, mass-flow rate of 1.5 g/s, and heating power of 120 kW/m^{2}K are shown in figs. 9 and 10. Consistent with the previous conclusions, external vibration does not influence the heat transfer process when the boundary-layer fuel has a temperature in the subcritical zone. When the boundary-layer fuel has a temperature in the pseudo-critical and supercritical zones, external vibration would reduce the wall temperature and thereby, enhance heat transfer. Therefore, under supercritical pressure conditions, external vibration mainly affects the heat transfer process through the boundary-layer. The boundary-layer fuel with a temperature in the pseudo-critical zone and supercritical zone is affected. However, the boundary-layer fuel with a temperature in the subcritical zone is not influenced.

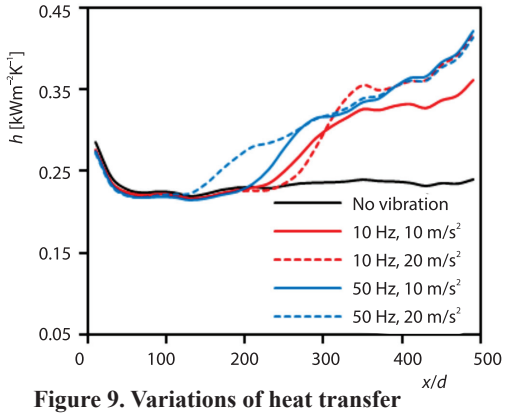

Figure 9. Variations of heat transfer coefficient along the flow direction (120 W/m^{2}K)

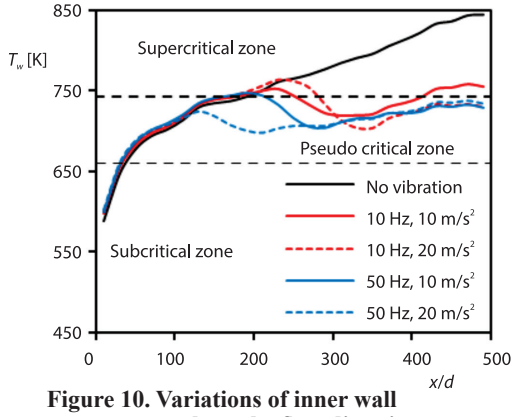

Figure 10. Variations of inner wall temperature along the flow direction (120 W/m^{2}K)

Influence of vibration on unstable flow heat transfer

The fuel temperature oscillation and wall temperature oscillation observed when the fluid has an inlet temperature of 293 K, a system pressure of 5 MPa, a mass-flow rate of 1.5 g/s, and a heat flux of 120 kW/m^2 are shown in fig. 11. Axial vibration is applied to the pipe to study whether external vibration has an influence on the oscillation process of this supercritical hydrocarbon fuel.

The variation can be divided into five phases on the timeline. In Phase a, there is no external vibration; in Phase b, external axial vibration with a frequency of 10 Hz and an amplitude of 10 m/s^2 exists; in Phase c, external axial vibration with a frequency of 10 Hz and an amplitude of 20 m/s^2 exists; in Phase d, external axial vibration with a frequency of 50 Hz and an amplitude of 10 m/s^2 exists; and in Phase e, external axial vibration with a frequency of 50 Hz and an amplitude of 20 m/s^2 exists. The influence of vibration on fuel temperature is shown in tab. 2. It can be considered that external vibrations of different frequencies and acceleration amplitudes have different influences on the instability of fuel flow. High frequency

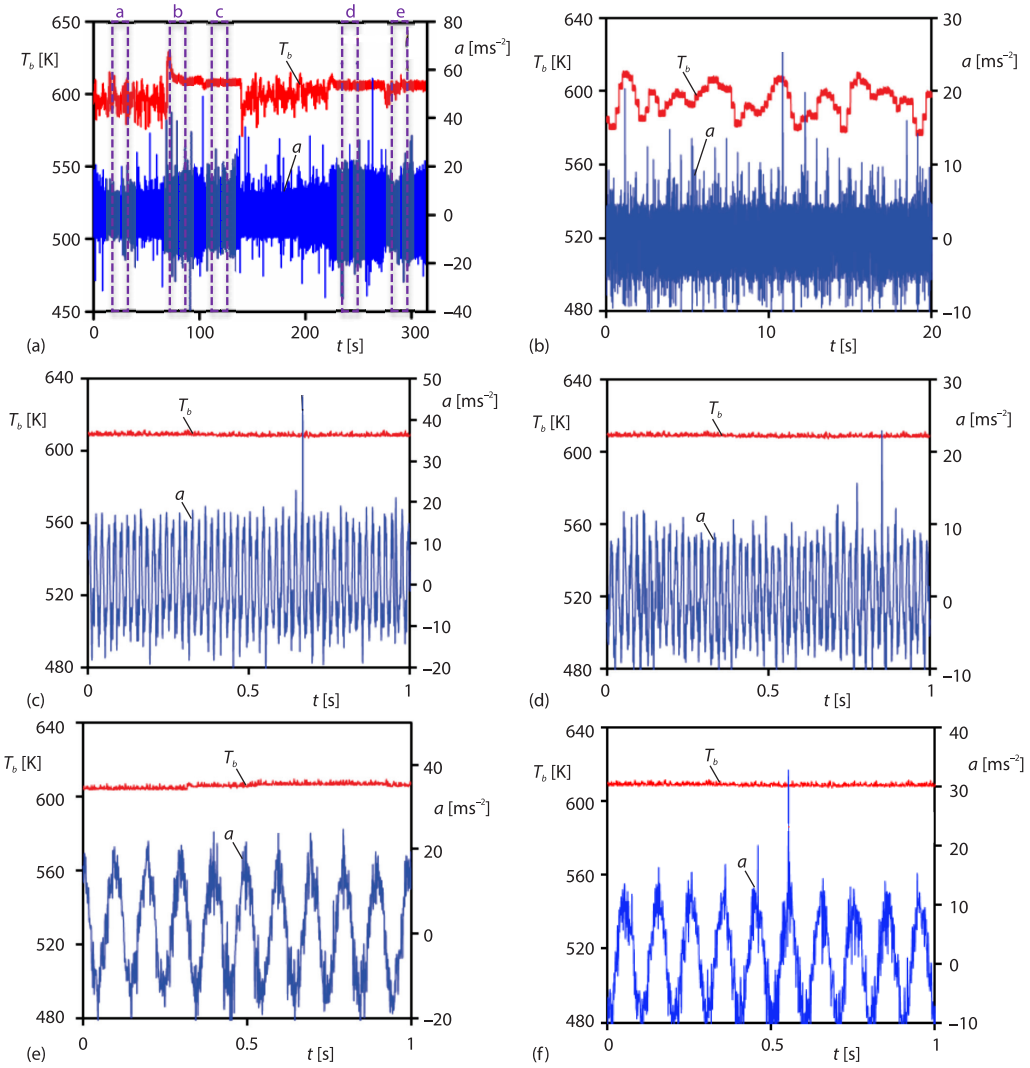

Figure 11. The unsteady flow under supercritical pressure condition (=1.5 g/s, H = 120 kW/m2K, P = 5 MPa); (a) outlet fuel temperature oscillation and pipe vibration, (b) Phase a, (c) Phase b, (d) Phase c, (e) Phase d, and (f) Phase e

vibration stabilizes the fuel at a relatively higher temperature, whereas low frequency vibration stabilizes the fuel at a relatively lower temperature. The amplitude of vibration acceleration has a negligible effect on stable fuel heat transfer.

Table 2. The influence of vibration on temperature oscillation of supercritical hydrocarbon fuel

	Amplitude [ms^{-2}]	Frequency [Hz]	Average fuel temperature [K]	Oscillation amplitude [K]
Phase a	0	0	600	40
Phase b	10	10	610	0
Phase c	20	10	610	0
Phase d	10	50	605	0
Phase e	20	50	610	0

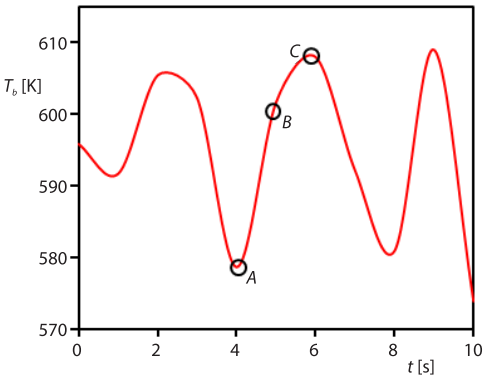

Figure 12. The exit fuel temperature of unsteady flow at supercritical pressure

The outlet fuel temperature at the three instants A, B, and C can reflect the oscillation information of the fuel temperature in one cycle. As shown in fig. 12, when external vibrations with a frequency of 10 Hz and vibration acceleration of 20 m/s^2 or those with a frequency of 50 Hz and vibration acceleration of 20 m/s^2 are applied to the pipe, the dynamic process of the influence of external vibration on the thermoacoustic oscillation in a cycle can be studied by the distribution patterns of fuel temperature, temperature of the inner wall surface, heat transfer coefficient, and Reynolds number along the length at A, B, and C.

The variation in the inner wall temperature along the flow direction is shown in fig. 13. The external vibration suppresses the instability of the flow and thereby, ensures that the inner wall temperature is stable along the length. Furthermore, there is a significant decrease in the wall temperature. When the external vibration frequency is 10 Hz, the wall temperature begins to decrease at $x/d = 350$ and recovers at the outlet. When the external vibration frequency is 10 Hz, the wall temperature begins to decrease at $x/d = 210$ and recovers at the outlet. Figure14 shows the variation in the main flow temperature along the flow direction. It is observed that external vibration maintains the main flow temperature at the vibration-free peak value.

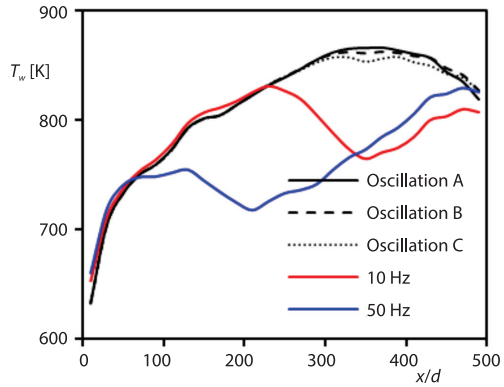

Figure 13. Variations of inner wall temperature along the flow direction

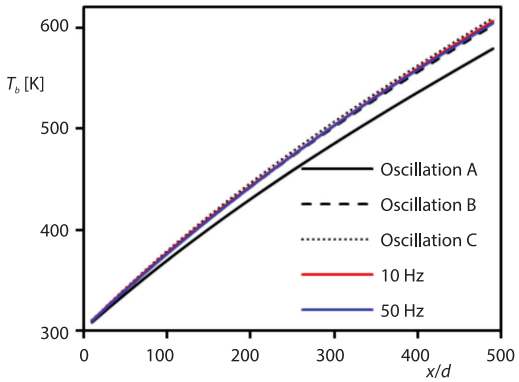

Figure 14. Variations of fuel temperature along the flow direction

The influence of external vibration on the boiling oscillation heat transfer coefficient is shown in fig. 15. The figure shows that external vibration would enhance heat transfer. The higher the vibration frequency, the higher is the enhancement of heat transfer. Figure 16 shows the variation in the Reynolds number along the length. It is observed that the Reynolds number under external vibration conditions remains at the vibration-free peak value. Because the Reynolds number is below 4500 along the length, the flow conditions have negligible influence on heat transfer.

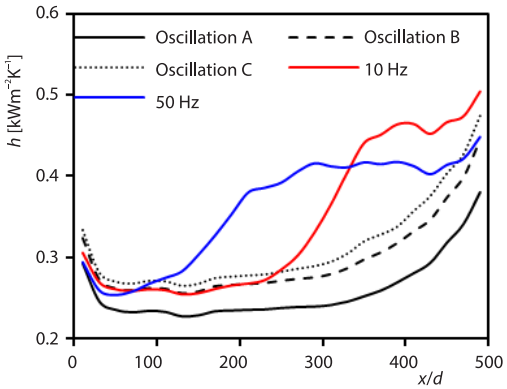

Figure 15. Variations of inner wall temperature along the flow direction

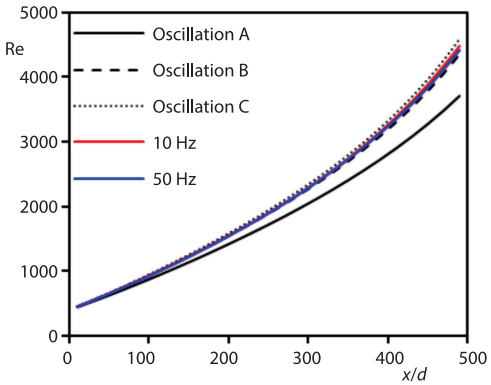

Figure 16. Variations of fuel temperature along the flow direction

Conclusions

The influence of vibration on the flow and heat transfer of the cooling channel was investigated by experiments in this study. Special attention was paid to the variations in the pseudo-critical zone and supercritical zone. The conclusions are as follows.

- With a supercritical pressure, the external vibration would enhance the flow and heat exchange of the cooling channel only when the fuel temperature is below the critical temperature and the inner wall temperature is above the critical temperature.
- With a supercritical pressure, vibration would suppress unstable flow and enhance heat transfer.

Reference

[1] Zhang, J. L., *et al.*, Investigations on Flame Liftoff Characteristics in Liquid-kerosene Fueled Supersonic Combustor Equipped with Thin Strut, *Aerospace Science and Technology*, *84* (2019), Jan., pp. 686-697
[2] Srinivasan, K., *et al*., Supersonic Combustion of A Scramjet Engine Using Hydrogen Fuel in Shock Tunnel, *AIAA*, *56* (2018), 9, pp. 3600-3609
[3] Ma, J. C., *et al*., Control-Oriented Unsteady 1-D Model for A Hydrocarbon Regeneratively-Cooled Scramjet Engine, *Aerospace Science and Technology*, *85* (2019), Feb., pp. 158-170
[4] Gascoin, N., *et al*., Validation of Transient Cooling Modelling for Hypersonic Application, *Journal of Thermophysics and Heat Transfer*, *21* (2007), 1, pp. 86-94
[5] Qin, A., *et al*., Multi-Objective Optimization on Regenerative Cooling Structure of Scramjet, *Journal of Propulsion Technology*, *39* (2018), 6, pp. 136-144
[6] Zhang, S. L., *et al.*, Review on Regenerative Cooling Technology of Hypersonic Propulsion, *Journal of Propulsion Technology*, *39* (2018), 10, pp. 23-36
[7] Han, Y., *et al*., Assessment of a Hybrid RANS/LES Simulation Method and URANS Method in Depicting the Unsteady Motions of Flow Structures in a Scramjet Combustor, *Aerospace Science and Technology*, *72* (2018), Jan., pp. 114-122
[8] Liu, Z., *et al*., Convective Heat Transfer and Pressure Drop Characteristics of Near-Critical-Pressure Hydrocarbon Fuel in a Minichannel, *Applied Thermal Engineering*, *51* (2013), 1-2, pp. 1047-1054
[9] Kafengauz, N. L., Fedorov, M. I., Pseudoboiling and Heat Transfer in a Turbulent Flow, *Journal of Engineering Physics*, *14* (1968), 5, pp. 489-490
[10] Linne, D. L., *et al.*, Evaluation of Heat Transfer and Thermal Stability of Supercritical JP-7 Fuel, *Proceedings*, 33th Joint Propulsion Conf. and Exhibit, Seattle, Wash., Usa, 1997, pp. 1997-3041
[11] Zhou, W., *et al*., Mechanism and Influencing Factors Analysis of Flowing Instability of Supercritical Endothermic Hydrocarbon Fuel Within a Small-Scale Channel, *Applied Thermal Engineering*, *71* (2014), 1, pp. 34-42

[12] Wang, H., *et al*., Experimental Investigation on the Onset of ThermoAacoustic Instability of Supercritical Hydrocarbon Fuel Flowing in a Small-Scale Channel, *Acta Astronaut*, *117* (2015), Dec., pp. 296-304
[13] Wang, H., *et al*., Experimental Investigation on the Characteristics of Thermo-Acoustic Instability in Hydrocarbon Fuel at Supercritical Pressures, *Acta Astronaut*, *121* (2016), Apr., pp. 29-38
[14] Zan, H., *et al.*, Investigation on Thermo-Acoustic Instability Dynamic Characteristics of Hydrocarbon Fuel Flowing in Scramjet Cooling Channel Based on Wavelet Entropy Method, *Acta Astronautica*, *147* (2018), June, pp. 27-36
[15] Zan, H., *et al*., Recurrence Network Analysis for Uncovering Dynamic Transition of Thermo-Acoustic Instability of Supercritical Hydrocarbon Fuel Flow, *Aerospace Science and Technology*, *85* (2019), Feb., pp. 1-12
[16] Han, Y., *et al*., Assessment of a Hybrid RANS/LES Simulation Method and URANS Method in Depicting the Unsteady Motions of Flow Structures in a Scramjet Combustor, *Aerospace Science and Technology, 72* (2018), Jan., pp. 114-122
[17] Ma, F., *et al*., Thermoacoustic Flow Instability in a Scramjet Combustor, *Proceedings*, 41st AIAA/ASME/SAE/ASEE Joint Propulsion Conference & Exhibit, Tucson, Ariz., USA, 2005, p. 3824
[18] Guo, C. H., *et al*., Effect of Mechanical Vibration on Flow and Heat Transfer Characteristics in Rectangular Microgrooves, *Applied Thermal Engineering*, *52* (2013), 2, pp. 385-393
[19] Soong, C. Y., *et a*l., An Experimental Study of Convective Heat Transfer in Radially Rotating Rectangular Ducts, *Journal of Heat Transfer*, *113* (1991), 3, pp. 604-611
[20] Benhamou, B., *et al*., Transient Effects of Orthogonal Pipe Oscillations on Laminar Developing Incompressible Flow, *International Journal for Numerical Methods in Fluids*, *34* (2000), 7, pp. 561-584
[21] Benhamou, B., *et al*., Periodic Characteristics of Laminar Developing Flow Through a Horizontal Tube Subject to Radial Oscillations, *Transactions of the Canadian Society for Mechanical Engineering*, *26* (2002), 2, pp. 219-239
[22] Xie, F., *et al*., The Flow Dynamics of the Garden-hose Instability, *Journal of Fluid Mechanics*, *800* (2016), Aug., pp. 595-612
[23] Mittal, S., Kumar, B., Flow Past a Rotating Cylinder, *Journal of Fluid Mechanics*, *476* (2003), Feb., pp. 303-334
[24] Zhou, W. J., *et al*., Experimental Study on Effect of Pressure on Heat Sink of n-Decane, *Chemical Engineering Journal*, *243* (2014), May, pp. 127-136
[25] Han, Z., *et al*., Experimental Investigation on Heat Transfer of n-Decane-ZnO Nanofluids in a Horizontal Tube under Supercritical Pressure, *International Communications in Heat and Mass Transfer*, *121* (2021), Feb., 105108
[26] Fu, Y. C., *et al*., Experimental Investigation on Convective Heat Transfer of Supercritical RP-3 in Vertical Miniature Tubes with Various Diameters, *International Journal of Heat and Mass Transfer*, *121* (2017), Sept., pp. 814-824

Paper submitted: July 6, 2021
Paper revised: August 2, 2021
Paper accepted: August 8, 2021